RSC Advances

PAPER

View Article Online
View Journal | View Issue

Cite this: *RSC Adv.*, 2014, **4**, 46680

Novel design approaches for multifunctional information carriers†

Melanie Ecker and Thorsten Pretsch*

Received 20th August 2014
Accepted 17th September 2014

DOI: 10.1039/c4ra08977d

www.rsc.org/advances

Two design approaches for multifunctional information carriers are introduced. In the first one, quick response (QR) code carriers, which were composed of poly(ester urethane) (PEU) and microencapsulated thermochromic pigments (T-PIGs), differing in color and color switching temperature (CST), were prepared. The obtained material systems exhibited machine-readable QR codes at 23 °C and a two-stage decolorization when heated, culminating in unreadable QR codes at temperatures above the highest CST of the employed T-PIGs. In the second scenario, information carriers were sealed with a dark, thermochromic PEU layer. As a result, the QR codes were hidden at 23 °C and became readable upon heating due to color fading. Beyond the characterization of the employed components, preparation methods, functionality analyses and durability investigations are reported. When heated after thermo-mechanical programming, pronounced shape memory properties could be verified. The thermo-responsiveness of such multifunctional material systems may qualify them for usage in anti-counterfeiting applications.

Introduction

After being quasi plastically distorted, shape memory polymers (SMPs) are able to recover their original shape when an appropriate external stimulus is applied.[1–3] Conventionally, the process of transferring a polymer to a temporary shape is called "programming". Therefore, the SMP is heated above a characteristic phase transition temperature T_{trans}, deformed and cooled under constraint conditions to the shape fixity temperature. As a result, the polymer chains are stabilized in a state of low conformational entropy.[4,5] Once heated again above T_{trans}, the gain in entropy drives shape recovering.

The structural prerequisite for shape memory behavior is a network architecture based on net points which are interconnected by switching segments. Usually, the net points are formed by chemical or physical cross-links and determine the permanent shape of the polymer. In turn, the switching segments are sensitive to external stimuli and serve as a mobile phase.

Physically cross-linked, phase segregated block copolymers like poly(ester urethanes) (PEUs) belong to the most promising SMP families.[6–12] Depending on the applied programming route, switching can be accomplished when passing the glass transition ($T_{trans} = T_g$) or the melting transition ($T_{trans} = T_m$) of the polyester soft segment.[13,14] Advantageously, T_{trans} can be synthetically adjusted in a wide temperature range by changing the molecular weight of the soft segment and thereby the crosslink density.[15–19] Post-polymerization cross-linking of structural motifs, which are part of the polymer repeat units, by curing[20] or electron beam irradiation[21] is another promising way to control the thermal and mechanical properties of polyurethane SMP systems. Besides that, temperature-memory effects open the door to precisely set transition temperatures within a phase transition region without the need of structural modification.[22,23]

Inspired by potential applications for SMPs such as textiles[24,25] and medical devices,[26–28] fundamental research started focusing on multifunctional polymers and their composites, which are characterized by the coexistence of shape memory properties and at least one further functionality.[29,30] Fruitful examples of such polymer systems are electroactive[31–38] or magnetoactive[39–41] SMP composites same as biodegradable SMPs[42–49] and color-changing SMPs.[50,51] In terms of latter, multifunctionality was verified by Wu *et al.* who reported on the synthesis and characterization of a PEU, in which chromic dye units of tetraphenylethylene were covalently attached to poly(ε-caprolactone), serving as soft segment. As a result of aggregation and disaggregation phenomena, a memory chromic behavior could be realized.[51] Kunzelman *et al.* performed

BAM Federal Institute for Materials Research and Testing, Polymers in Life Science and Nanotechnology, Division 6.5, Unter den Eichen 87, 12205 Berlin, Germany. E-mail: thorsten.pretsch@bam.de

† Electronic supplementary information (ESI) available: ATR-FTIR spectra of melamine, T-PIG blue-43 and T-PIG magenta-43, including band assignments, images of differently colored, solvent cast PEU films, microscopic images of solvent cast PEU films, DSC thermogram of a programmed type 1 QR code carrier, CIELAB values and color differences of a type 1 QR code carrier, microscopic image of a type 2 QR code carrier and its temperature-dependent Michelson contrast, photographs of type 1 and type 2 QR code carriers before and after running 100 temperature cycles, CIELAB values of a type 1 QR carrier after thermal cycling. See DOI: 10.1039/c4ra08977d

pioneering work by integrating excimer-forming fluorescent chromophores *via* guest diffusion into a chemically cross-linked poly(cyclooctene) (PCO) matrix.[50] In the obtained phase-separated blends, color changes of the chromogenic dye resulted from self-assembly or dispersion of dye molecules. Another way to obtain SMP systems with thermoreversible color changes is to integrate functional microcapsules containing color-forming components in a polymer matrix. Following this approach, our group recently used a two-step process to obtain quick response (QR) code carriers, characterized by mutually complementing thermochromic and shape memory properties.[52] Therefore, laminate structures were prepared by solvent casting of thin polymer films doped with thermochromic pigments (T-PIGs) atop a PEU substrate. After drying on air, machine-readable QR codes were engraved in the cover layer. The employed T-PIGs were built up by a mixture of leuco-dye, a color-developer and a solvent; the coloring components were microencapsulated in a polymeric shell. Such systems are known to change their color thermoreversibly due to electronic interaction between the dye and dye-developer, which is inhibited upon melting and allowed upon crystallization of the solvent.[53–57]

Herein, we introduce information carriers, which contain two sorts of T-PIGs, differing in room temperature color and color switching temperature (CST). Depending on the preparation method, a mixture of T-PIGs was distributed in the same PEU matrix atop PEU substrate before QR code carriers were prepared by laser engraving and cutting or T-PIGs were separately embedded in different layers atop PEU substrate at which a QR code carrying bottom layer was completely covered by a continuous layer. The aim of this work is to investigate their functionality. Here, one focus was on the thermo-reversibility of color changes and the associated changes in surface contrast, which were directly affecting the machine-readability of the QR codes. In a further step, programming was applied and the shape memory behavior investigated. Against this background, a discussion of the obtained results is provided.

Experimental section

Preparation methods

Desmopan DP 2795A SMP, which is a PEU from Bayer MaterialScience AG, was used as received. The hard segments were composed of 4,4′-methylenediphenyl diisocyanate and 1,4-butanediol as chain extender, whereas the soft segments were based on poly(1,4-butylene adipate) (PBA). Detailed information regarding the two-step synthesis process is given in a patent.[58] The raw material was supplied both as pellets, foil[59] and injection molded plaques, latter with dimensions of 126 mm × 52 mm × 2 mm.

Microencapsulated thermochromic pigments (T-PIGs) were purchased as powder from Sintal Chemie GmbH. The obtained T-PIGs varied in room temperature color and CST. The T-PIGs were black, blue and magenta (CST = 43 °C) and orange, green and magenta (CST = 65 °C). Accordingly, they were termed "T-PIG black-43", "T-PIG blue-43", "T-PIG magenta-43", "T-PIG organge-65", "T-PIG green-65" and "T-PIG magenta-65".

Table 1 T-PIG mixtures, which were used for paste preparation, and the associated colors of the pastes

First component	Second component	T-PIG mixture	Color at 23 °C
T-PIG black-43	T-PIG orange-65	#1	Brown
T-PIG blue-43	T-PIG green-65	#2	Petrol green
T-PIG magenta-43	T-PIG orange-65	#3	Red
T-PIG blue-43	T-PIG magenta-65	#4	Purple

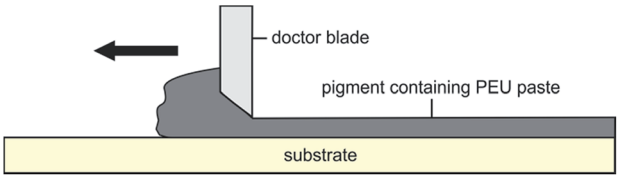

Fig. 1 Schematic setup and functional principle of a doctor blade. The employed substrate was either glass or PEU.

The preparation of thermochromic polymer pastes was carried out as follows. At first, either 1.25 g of T-PIG or 2.5 g of a 1 : 1 mixture of two T-PIGs was suspended in 5 ml of *N*-methyl-2-pyrrolidone (NMP). After sonication for about 10 min at 23 °C, the dispersed T-PIGs were added to a solution, in which 5 g of PEU pellets or foil were dissolved in 15 ml of NMP. The resulting pastes were stirred for 5 min at 23 °C in order to obtain homogenous dispersions of the T-PIGs. This way, pastes containing different T-PIG mixtures were prepared, and their colors at 23 °C could be set by varying the combination of the individual components (Table 1).

Following a solvent cast approach, thin thermochromic polymer films were prepared by layering the pastes atop glass plates. Subsequently, a custom-built doctor blade[60] (Fig. 1) was used to remove the excess paste and obtain a homogenous layer thickness.

After solvent evaporation, the thermal and colorimetric properties of the films were studied. Depending on the selected paste, the content of T-PIGs inside the PEU films was 20 wt% in case of pastes containing one sort of T-PIG and 33 wt% when T-PIG mixtures were used.

The preparation of multifunctional information carriers was either carried out in two or three steps; accordingly, the obtained information carriers were denoted as "type 1" or "type 2" QR code carriers (Fig. 2). In both cases, a solvent cast approach was followed. This time, the above-mentioned pastes were distributed by means of a doctor blade (Fig. 1) atop a 2 mm thick PEU plate, which served as a substrate (step 1 in Fig. 2). After solvent evaporation for about 18 h at 23 °C, tightly connected laminate structures were obtained.

In a second step, a QR code (version 1, error correction level L)[61] carrying the encoded information "http://www.bam.de" was generated,[62] engraved in the pigment-containing PEU layer and type 1 QR code carriers were prepared by laser ablation and cutting with a 30 W CO_2 laser (step 2 in Fig. 2). By standard, the edge length of the QR code symbols was 14 mm at a quiet zone

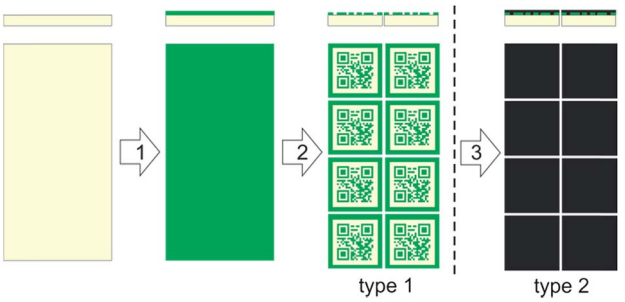

Fig. 2 Preparation scheme for QR code carriers (side view above and top view below). Type 1 QR code carriers were prepared by solvent casting of a first T-PIG containing PEU layer atop pristine PEU (step 1), laser engraving of a QR code pattern and cutting (step 2). To prepare type 2 QR code carriers, the aforementioned steps were applied and a surface-sealing layer containing T-PIG black-43 was deposited before cutting (step 3).

width of 1 mm. In order to ensure a sufficiently high surface contrast at 23 °C between the pigment-containing regions and the PEU substrate, a laser ablation depth of (120 ± 5) μm was selected.

The preparation of type 2 QR code carriers was realized in three steps (Fig. 2). In contrast to the above-described route, PEU pastes containing only one sort of T-PIG (CST = 65 °C) were selected in step 1 (Fig. 2). After laser engraving a QR code pattern into the cover layer (step 2 in Fig. 2), an information carrier with a machine-readable QR code was obtained as an intermediate form. Adjacently, the QR code carrying site of the information carrier was sealed with a paste containing T-PIG black-43 (step 3 in Fig. 2). In a final step, QR code carriers were cut out and dried on air for 36 h at 23 °C.

Characterization methods

The shape and size distribution of the T-PIGs was studied with a scanning electron microscope (SEM). The employed Zeiss Gemini Supra 40 device operated at an extra high tension of 10 kV. In order to ensure that the surface of T-PIGs was electrically conductive, a few nanometers thin carbon layer was deposited atop the microcapsules by means of a sputtering system. The size distribution of the T-PIGs was determined from scanning electron micrographs using the software program ImageJ.[63]

Differential scanning calorimetry (DSC) was used to study solvent cast PEU films. The films had a uniform thickness of (65 ± 5) μm and were either composed of PEU or PEU, which was loaded with one sort of T-PIG or mixtures therefrom. The measurements were conducted three days after film preparation with a DSC 7020 from Seiko Instruments. Initially, a sample, weighing approximately 5 mg, was sealed in an aluminum pan, before it was placed inside the calorimeter. The sample was cooled down to −90 °C and heated to 90 °C, before cooling and heating were repeated. All measurements were carried out with cooling and heating rates of 10 °C min^{-1}. For some of the obtained thermograms, a melting peak deconvolution was carried out with the Lorentz fit function of Origin 8.5.1 software.

The surface contrast of the QR code carriers was determined at different temperatures. Therefore, heating was applied and color photos were taken. Later, the pictures were converted into grayscale histograms by using the analysis program ImageJ. From these images the Michelson contrast C_M,[64] which is defined as the relation between the difference and the sum of the highest and lowest luminance L_{max} and L_{min}, differing in grayscale value, was calculated. For this purpose, the T-PIG containing areas and laser-ablated regions (PEU substrate) of the QR code carriers were considered. In detail, C_M was determined for five different subzones within the QR code area (top left, top right, center, bottom left and bottom right) and adjacently averaged. The maximum deviation from the mean value was determined and set as error.

The programming of information carriers was carried out with an MTS Insight 10 electromechanical testing system, which was equipped with a Thermcraft thermochamber. In accordance with the geometry of the QR code carriers, the recently introduced compressive deformation-determinated functionalization method was selected.[65] In the course of programming, a QR code carrier was positioned in the center between two pressure plates and an initial force of −10 N was applied to assure that the sample did not change position. Adjacently, the information carrier was heated with 4.3 °C min^{-1} to 80 °C and thus above the DSC melting peak offset temperature of the PBA phase, which was close to 50 °C.[65] After 5 min at 80 °C, the QR code carrier was loaded with a crosshead displacement rate of 0.5 mm min^{-1} until a maximum force F_{max} of 2.25 kN was achieved. In order to fix the temporary shape, F_{max} was maintained during cooling with 5.3 °C min^{-1} to −20 °C and thus below the DSC crystallization offset temperature of the PBA phase transition (≈−10 °C).[65] After 5 min at −20 °C, programming was finalized by unloading with a rate of 0.5 kN min^{-1}. In a last step, the QR code carrier was heated to 23 °C.

To follow the thermo-reversibility of color changes and to investigate the shape recovery behavior, programmed information carriers were gradually heated in the thermochamber from 23 to 70 °C, before they were cooled to 23 °C. In those temperature regions, in which distinct changes in color and shape occurred, namely around the CST of the T-PIGs and the melting transition of the PBA phase, heating and cooling steps of 2 °C were implemented. In the other regions, temperature intervals of 3 °C were chosen. In every case, the holding time at the different temperatures was 5 min. In parallel to temperature variation, color photos were taken using a Nikon D90 with macro objective. In order to ensure comparable conditions, the distance between the camera and the information carrier, the aperture, exposure time, focal length, ISO settings and white balance were set to be constant during the whole picture series. During shape recovering, the evolution of distorted QR code areas was followed with the image analysis program ImageJ. In scaled photographs, which were taken at different temperatures, the areas of the QR codes were obtained through manually fitting polygons to their boundary edges (Fig. 3). Temperature-dependent changes in QR code area were calculated as the difference $\Delta A = A_1 - A_0$ with A_0 being 256 mm^2. For error determination, the standard deviation was calculated for three measurements, which were carried out on the same QR code carrier.

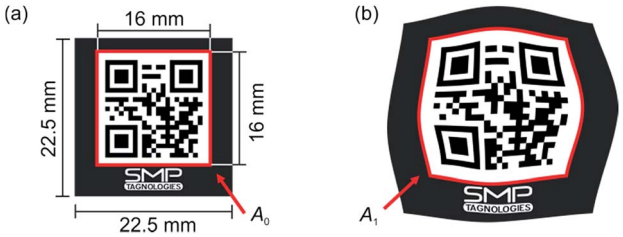

Fig. 3 Schematic illustration of a QR code carrier in the permanent shape (a) and after programming (b). The red lines surround those surface areas, which were considered when investigating shape memory properties. The state of the QR code carrier on the left largely corresponds to the recovered state.

The machine-readability of freshly prepared, programmed and recovered QR code carriers was investigated with a Samsung Galaxy S I9300 smartphone, equipped with the software "Barcode Scanner" version 4.7.0 from ZXing.[66] Commonly, the QR codes were scanned at 23, 50 and 70 °C. Thus, temperatures below, between and above the CSTs of the employed T-PIGs were selected.

For durability investigations, type 1 and type 2 QR code carriers were prepared and temperature cycled in a Thermcraft thermochamber for $N = 100$ times between 23 and 70 °C. The selected heating and cooling rates were 20 °C min^{-1}.

Results and discussion

Initially, the T-PIGs, which were differing in color at 23 °C and in color switching temperature (CST), were examined. As suggested by ATR-FTIR investigations, their polymeric shells were composed of melamine resin (ESI Fig. S1†). Subsequently, scanning electron microscopy was used to further examine the T-PIGs. Here, all T-PIGs were characterized by similar size distributions and mean particle sizes; two sorts of T-PIGs are exemplarily shown in Fig. 4.

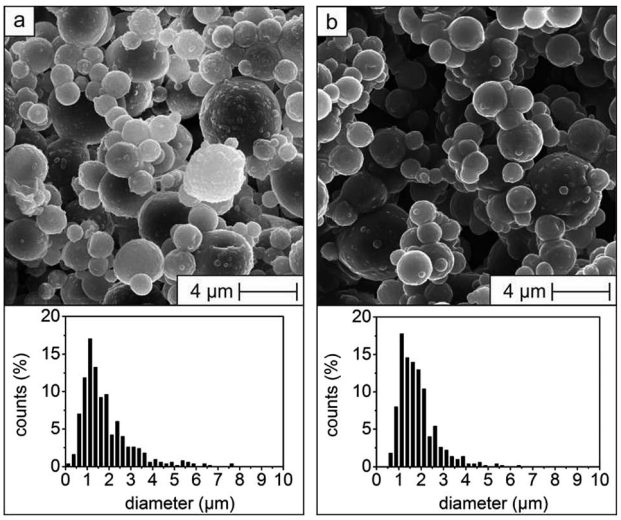

Fig. 4 Scanning electron micrographs of T-PIG blue-43 (a) and T-PIG magenta-65 (b) and the corresponding size distributions of the microcapsules.

Due to the similarities in shape and chemical structure, homogenous mixtures of two T-PIGs could be easily formed and a good dispersion be realized in polymer pastes, which were then used to prepare solvent cast PEU films (ESI Fig. S2†). The thickness of films, containing either one sort of T-PIG or mixtures of two T-PIGs, could be set in between (30 ± 5) and (150 ± 5) µm (ESI Fig. S3†) by means of a doctor blade (Fig. 1). By varying the mixtures of the T-PIGs (Table 1), polymer systems with different room temperature colors (brownish, petrol greenish, reddish and purplish) could be obtained (ESI, Fig. S2†).

In a next step, the thermal properties of the films were examined with the aid of differential scanning calorimetry (Fig. 5). When investigating PEU films without fillers, broad endothermic and exothermic signals with peak temperatures at 54 and 11 °C were detected and assigned to the melting and crystallization of poly(1,4-butylene adipate) (PBA).[52,65,67] Upon integrating T-PIG in the PEU matrix, the position of the melting signal nearly did not change, but the crystallization peak temperature decreased from 11 to about 8 °C. Apparently, the pretty high filler contents retarded the crystallization process by

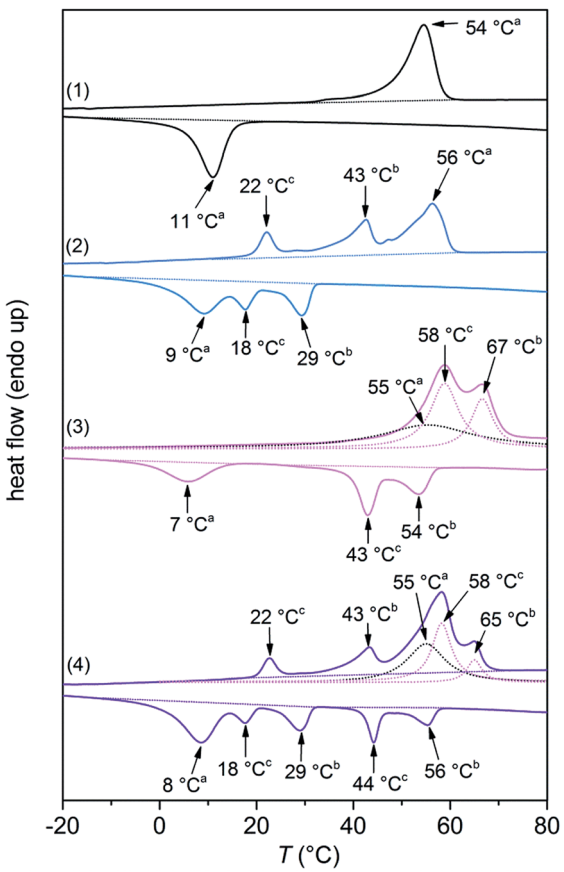

Fig. 5 DSC thermograms of a solvent cast PEU film (1) and solvent cast PEU films containing 20 wt% of T-PIG blue-43 (2), 20 wt% of T-PIG magenta-65 (3) and T-PIG mixture #4 (4, also see Table 1). In every single measurement, the first heating is plotted above the first cooling run. The signals were denoted as "a" (PBA phase changes), "b" (solvent-related phase changes) and "c" (phase changes associated with the color-developer).

hindering the diffusion of polymer chains to the growing crystallites. Under isothermal conditions, a similar behavior is known from other aliphatic polyesters like poly(ε-caprolactone) (PCL), which in the presence of organically modified clay shows delayed crystallization at higher filler contents.[68] In turn, under non-isothermal conditions, crystal growth is also retarded in Nylon 6 nanocomposites with high clay contents.[69]

The remaining DSC signals – some of them were obtained from peak deconvolution – could be attributed to the melting and crystallization of the color-developer and the solvent inside the polymeric microcapsules (Fig. 5). Independent of the employed T-PIGs, the melting of the solvent occurred at higher temperatures compared with the corresponding crystallization event. Indeed, both peak temperatures were separated by 14 °C (T-PIG blue-43) and 13 °C (T-PIG magenta-65), respectively. The reason is that the formation of crystal nuclei is hindered in polymeric microcapsules; among others, solvent crystallization is known to be dictated by the size of the microcapsules.[70] It is noteworthy that PEU containing two sorts of T-PIGs shows a thermal behavior, which was expected from the individually loaded PEU films, thus qualifying T-PIG mixtures in a PEU matrix for consecutive color changes.

Hereafter, two types of QR code carriers are introduced. Both of them were characterized by two-step color change capabilities, but were mostly differing in those temperature regions, in which their QR codes were decipherable. Type 1 QR code carriers were prepared by solvent casting of PEU pastes containing T-PIG mixtures atop PEU plates, followed by QR code engraving and laser cutting (Fig. 2). In contrast to an earlier preparation route, in which the pigment-containing PEU paste was manually distributed atop the substrate,[52] the layer thickness could precisely be set with the doctor blade (Fig. 1). From the viewpoint of color saturation, layer thicknesses of (65 ± 5) μm turned out to be useful and were selected therefore (ESI, Fig. S4†).

The thermochromic behavior of the obtained type 1 QR code carriers was elucidated by heating from 23 to 70 °C. The selected T-PIG mixtures exhibited a similar thermochromic behavior in all QR code carriers investigated (Fig. 6). Typically, two-step color changes occurred, the first one at around 33 °C and the second one at about 60 °C. It is noteworthy that at temperatures above 57 °C, the QR codes became machine-unreadable. During an ensuing cooling, the colors returned at around 54 and 30 °C, respectively. A discrepancy between the temperatures of color fading and return is commonly detected in T-PIGs[71,72] and associated with the above-mentioned distinctions in solvent melting and crystallization behavior.

Moreover, contrast determinations were carried out at 23, 50 and 70 °C to follow the temperature dependence of Michelson contrast C_M, which, among others, is an adequate tool to gain information on the machine-readability of QR codes.[73] At ambient temperature, the comparatively highest C_M values could be detected (Table 2). Upon heating to 50 °C, the T-PIG with the lower CST completely decolorized and the residual color was determined by the T-PIG with the higher CST. In this stage, the surface contrast was still strong enough to read out the QR codes ($C_M \geq 0.22$). Further heating to 70 °C resulted in a

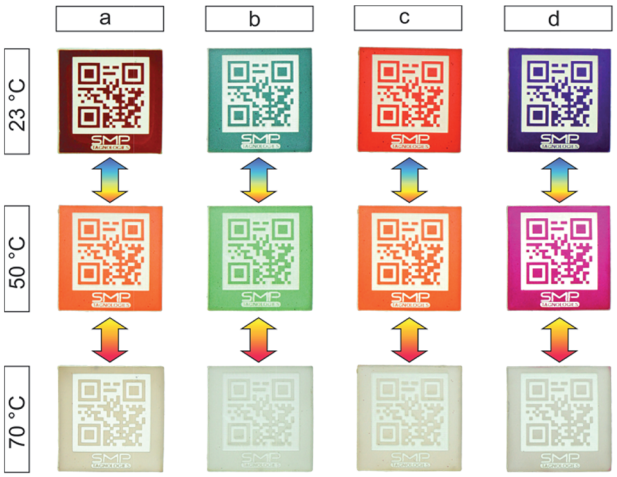

Fig. 6 Thermochromic behavior of permanent-shaped type 1 QR code carriers, which were surface-colored with T-PIG mixture #1 (a), #2 (b), #3 (c) and #4 (d). Due to the semicrystalline nature of the PBA phase at 23 °C, laser-ablated regions were whitish and contrasting the intensely colored T-PIG containing regions.

Table 2 Temperature dependence of Michelson contrast C_M of those thermochromic QR code carriers, which are exhibited in Fig. 6

	C_M (a)	C_M (b)	C_M (c)	C_M (d)
23 °C	0.79 ± 0.01	0.36 ± 0.02	0.34 ± 0.02	0.62 ± 0.05
50 °C	0.25 ± 0.02	0.26 ± 0.02	0.22 ± 0.01	0.31 ± 0.04
70 °C	0.09 ± 0.01	0.04 ± 0.01	0.04 ± 0.01	0.07 ± 0.01

complete discoloration of the T-PIG containing regions. Concomitantly, C_M dropped below a value of 0.1 and the QR codes became indecipherable. This interrelationship is in accordance with recent investigations on information carriers containing non-functional dye.[73] The thermo-reversibility of contrast changes and the return of QR code readability could be verified when cooling the information carriers back to 23 °C. In so far, selective contrast change capabilities could be detected.

In a next step, the shape memory behavior was investigated. First of all, type 1 QR code carriers were programmed. The selected programming method was based on compressive deformation and recently applied to other information carriers.[65] As a result, the information carriers could be stabilized in thermo-responsive states and their QR codes were randomly distorted and therefore indecipherable. A more detailed consideration gave that the QR code areas were enlarged by about 50% (schematically indicated in Fig. 3) and the thickness of the information carriers was reduced from (2.25 ± 0.02) to (1.78 ± 0.02) mm. Subsequently, the thermo-responsiveness was investigated as exemplified in Fig. 7 for a purplish type 1 QR code carrier. The corresponding changes in QR code area and Michelson contrast are given in Fig. 8.

As deducible from the image series, heating initiated color fading of the blue component (T-PIG blue-43) before shape recovering set in. Apparently, the solvent inside the microcapsules of T-PIG blue-43 started melting at 32 °C (Fig. 5). In turn,

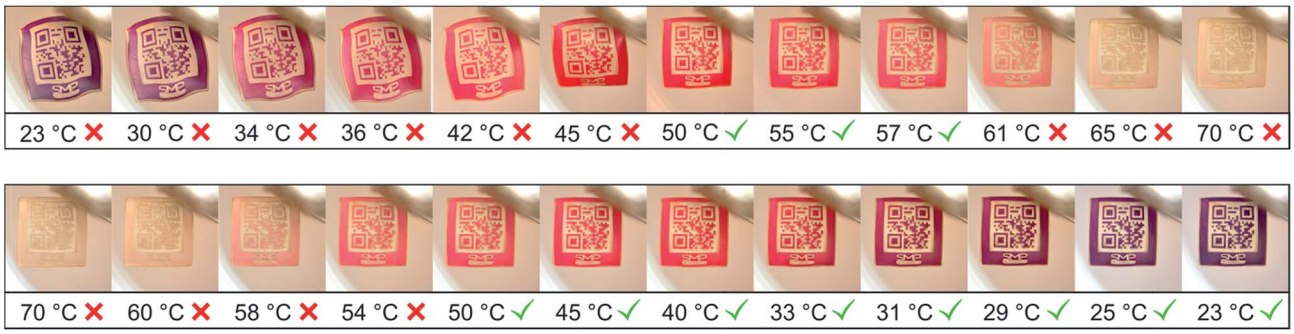

Fig. 7 Thermo-responsiveness of a type 1 QR code carrier which was surface-colored with T-PIG mixture #4. Starting with the programmed state, the information carrier was heated from 23 to 70 °C (image series above) and cooled to 23 °C (image series below). The symbols on the right side of the temperature values indicate, whether the QR codes were machine-readable or not.

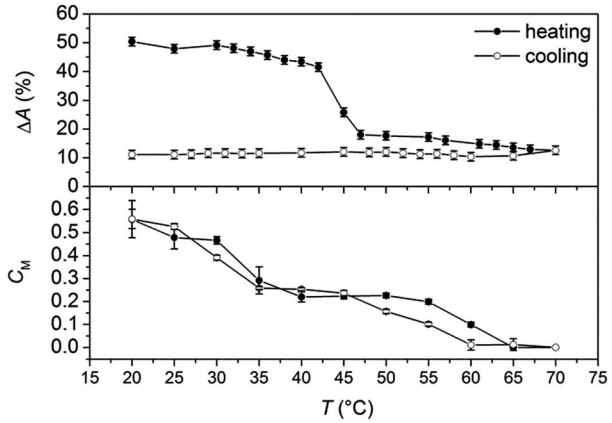

Fig. 8 Changes in QR code area ΔA (top) and Michelson contrast C_M (bottom), when heating and cooling a programmed type 1 QR code carrier, which was surface-colored with T-PIG mixture #4.

shape recovering was initiated at 42 °C. Since this value was on the outermost region of the PBA melting signal as detected for solvent cast PEU film (Fig. 5), shape recovering must have been dominated by the thermal behavior of the programmed PEU substrate. In fact, this could be proven by means of a further DSC heating scan on a sample of a programmed type 1 QR code carrier. In the respective thermogram, PBA melting was characterized by a broad endothermic signal, spreading from 30 to 53 °C (ESI Fig. S5†). At the activation temperature of the shape memory effect (42 °C), approximately 45% of the PBA crystallites were molten.

Upon further heating, the QR code pattern rectified and the QR code became decipherable at 50 °C. Above 60 °C, the magenta component decolorized. In parallel, the surface contrast decreased (C_M dropped below a value of 0.1, Fig. 8), which rendered the QR code unreadable. In the overall heating process, the QR code area decreased from 50.4% at 23 °C to 11.5% at 70 °C (Fig. 8).

Upon cooling, the magenta color reappeared at 52 °C, which was accompanied by a return in surface contrast and QR code readability. Finally, the purple color reappeared at about 30 °C. As expected, no significant changes occurred during cooling in the QR code area. The evolution in surface color was confirmed by temperature-dependent colorimetric measurements (ESI Fig. S6†). As evident in discrepancies regarding the evolution of all CIELAB values and color differences,[74,75] the color of the T-PIGs depended on whether heating or cooling was applied.[76] This behavior is in line with our DSC results, where the melting peaks of the solvent inside the microcapsules of the T-PIGs were found at higher temperatures compared with the respective crystallization signals.

To extend our concept of multifunctional information carriers, we followed one further design approach. For this purpose, a (119 ± 6) μm thick PEU layer containing 20 wt% of T-PIG green-65 was solvent cast atop a PEU plate, before a QR code was engraved and the QR code side sealed with a PEU layer containing T-PIG black-43 (Fig. 2). The resulting type 2 QR code carrier was microscopically investigated. The cover layer thickness was (211 ± 6) μm above laser ablated regions and (152 ± 6) μm in the remaining regions (ESI Fig. S7†). In a next step, the thermochromic behavior was examined (Fig. 9).

In contrast to those information carriers shown in Fig. 6, the QR code was hidden at 23 °C by the dark sealing layer. Upon heating to 70 °C, a machine-readable QR code appeared at 44 °C and disappeared at 62 °C. Upon cooling, the QR code was readable in between 58 and 32 °C.

In order to find out in how far programming affected the thermo-responsiveness, a type 2 QR code carrier was investigated. Fig. 10 shows that heating initiated color fading of the cover layer (T-PIG black-43) whereupon a distorted QR code became visible before shape recovering set in.

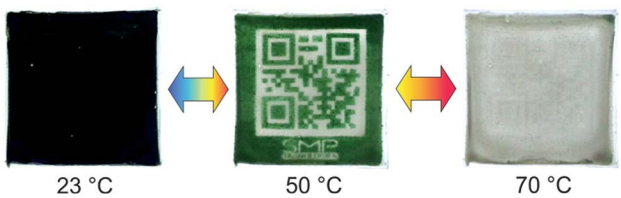

Fig. 9 Thermo-responsiveness of a permanent-shaped type 2 QR code carrier, containing a continuous layer of T-PIG black-43 atop a laser-engraved layer of T-PIG green-65.

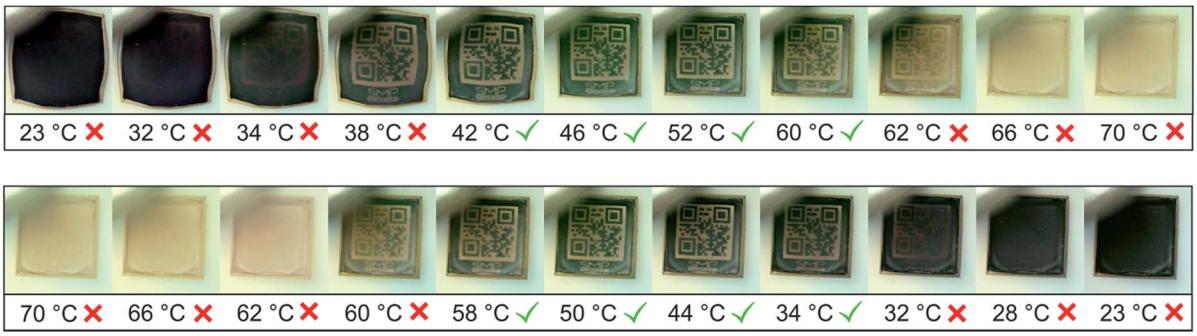

Fig. 10 Thermo-responsiveness of a type 2 QR code carrier containing T-PIG green-65 in a laser-engraved bottom layer and T-PIG black-43 in a cover layer. Starting with the programmed state, the information carrier was heated from 23 to 70 °C (image series above) and cooled to 23 °C (image series below). The symbols on the right side of the temperature values indicate, whether the QR codes were machine-readable or not.

At temperatures in between 42 and 60 °C, the QR code was in a machine-readable state. Upon further heating, the green layer decolorized and the QR code disappeared. During an ensuing cooling, a machine-readable QR code reappeared at 52 °C and was completely hidden at temperatures below 28 °C. It is noteworthy, that for type 2 QR code carriers the Michelson contrast was in general pretty low with maximum values of about 0.2 (ESI Fig. S8†). Obviously, the thermochromic top layer was not completely transparent above the CST of T-PIG black-43, which can be explained with a sensitivity toward light scattering on the employed microcapsules.[77]

Finally, we investigated the durability of our QR code carriers. Therefore, they were heated to 70 °C and adjacently cooled to 23 °C, before further 99 heating-cooling cycles were carried out (ESI Fig. S9†). As evidenced by spectrophotometric measurements, the temperature colors at 23 and 50 °C remained almost unaffected by thermal cycling (ESI Table S1†). Apart from that, color fading and regaining was found in the same temperature regions as for freshly prepared information carriers. This demonstrates that reliable color switching could be accomplished, which assured that those temperature areas, in which the QR codes were readable, could be retained.

Conclusions

Mixing of different sorts of T-PIGs in a PEU matrix established a fruitful basis to obtain multifunctional material systems with two-stage, thermoreversible color change capabilities. When studying the thermo-responsiveness of type 1 QR code carriers, their codes were visible at ambient temperature and became unreadable at temperatures above the highest decolorization temperature of the employed T-PIGs. Following another design approach, type 2 QR code carriers could be obtained. This time, QR codes were concealed at room temperature and became decipherable upon heating in a small temperature region. It is remarkable that after 100 heating-cooling cycles, no significant change in thermochromic behavior could be detected for both systems.

The verified functionalities add well to our existing portfolio of security features, which could render information carriers more difficult-to-copy, thus qualifying them as promising technology for product authentication and identification. The introduced QR code carriers can be used in a permanent or programmed state. Both could act as a deterrent to potential counterfeiters. In particular, changes in the choice of programming instruments may offer various modification possibilities.[78] Beyond that, the incorporation of more than two T-PIGs in one and the same polymer matrix or in multilayer polymer films may enhance the spectrum of color changes and could be a key to obtain highly functional information carriers.

Acknowledgements

The authors gratefully acknowledge financial support from the German Federal Ministry of Education and Research (BMBF, project funding reference number 03V0043). Sigrid Benemann is acknowledged for conducting SEM, Dietmar Neubert for DSC measurements and Josefine Buschke for taking the series of photographs. The authors thank Bayer MaterialScience AG (BMS) for kindly providing the PEU, Jürgen Hättig (BMS) for thoughtful discussions and Michael Maskos (Fraunhofer ICT-IMM) and Gerhard Wegner (Max Planck Institute for Polymer Research) for the support of this project and suggestions for future work.

Notes and references

1 A. Lendlein and S. Kelch, *Angew. Chem., Int. Ed.*, 2002, **41**, 2034–2057.
2 B. Dietsch and T. Tong, *J. Adv. Mater.*, 2007, **39**, 3–12.
3 C. Liu, H. Qin and P. T. Mather, *J. Mater. Chem.*, 2007, **17**, 1543–1558.
4 P. J. Flory, in *Principles of Polymer Chemistry*, Cornell University Press, Ithaca, New York, 1953, pp. 541–594.
5 L. R. G. Treloar, in *The Physics of Rubber Elasticity*, Oxford University Press, Oxford, 1975, pp. 24–41.
6 F. K. Li, X. Zhang, J. N. Hou, M. Xu, X. L. Lu, D. Z. Ma and B. K. Kim, *J. Appl. Polym. Sci.*, 1997, **64**, 1511–1516.
7 H. M. Jeong, S. Y. Lee and B. K. Kim, *J. Mater. Sci.*, 2000, **35**, 1579–1583.
8 S. J. Chen, J. L. Hu, C. W. M. Yuen, L. K. Chan and H. T. Zhuo, *Polym. Adv. Technol.*, 2010, **21**, 377–380.

9 Y.-C. Chung, D. K. Nguyen, J. W. Choi and B. C. Chun, *J. Appl. Polym. Sci.*, 2010, **120**, 2063–2073.
10 T. Pretsch and W. W. Müller, *Polym. Degrad. Stab.*, 2010, **95**, 880–888.
11 W. Wang, Y. Jin, P. Ping, X. S. Chen, X. B. Jing and Z. H. Su, *Macromolecules*, 2010, **43**, 2942–2947.
12 K. K. Julich-Gruner, C. Löwenberg, A. T. Neffe, M. Behl and A. Lendlein, *Macromol. Chem. Phys.*, 2013, **214**, 527–536.
13 F. L. Ji, J. L. Hu, T. C. Li and Y. W. Wong, *Polymer*, 2007, **48**, 5133–5145.
14 T. Pretsch, *Smart Mater. Struct.*, 2010, **19**, 015006.
15 P. Ping, W. Wang, X. Chen and X. Jing, *Biomacromolecules*, 2005, **6**, 587–592.
16 S. J. Chen, J. L. Hu, Y. Q. Liu, H. M. Liem, Y. Zhu and Q. H. Meng, *Polym. Int.*, 2007, **56**, 1128–1134.
17 S. Mondal and J. L. Hu, *J. Elastomers Plast.*, 2007, **39**, 81–91.
18 D. Ratna and J. Karger-Kocsis, *J. Mater. Sci.*, 2008, **43**, 254–269.
19 M. Bothe, F. Emmerling and T. Pretsch, *Macromol. Chem. Phys.*, 2013, **214**, 2683–2693.
20 K. Hearon, K. Gall, T. Ware, D. J. Maitland, J. P. Bearinger and T. S. Wilson, *J. Appl. Polym. Sci.*, 2011, **121**, 144–153.
21 K. Hearon, C. J. Besset, A. T. Lonnecker, T. Ware, W. E. Voit, T. S. Wilson, K. L. Wooley and D. J. Maitland, *Macromolecules*, 2013, **46**, 8905–8916.
22 K. Kratz, U. Voigt and A. Lendlein, *Adv. Funct. Mater.*, 2012, **22**, 3057–3065.
23 N. Fritzsche and T. Pretsch, *Macromolecules*, 2014, **47**, 5952–5959.
24 J. Hu, in *Shape-Memory Polymers and Multifunctional Composites*, ed. J. Leng and S. Du, CRC Press, 2010, pp. 293–313.
25 J. Hu, H. Meng, G. Li and S. I. Ibekwe, *Smart Mater. Struct.*, 2012, **21**, 053001.
26 F. E. Feninat, G. Laroche, M. Fiset and D. Mantovani, *Adv. Eng. Mater.*, 2002, **4**, 91–104.
27 K. Gall, C. M. Yakacki, Y. P. Liu, R. Shandas, N. Willett and K. S. Anseth, *J. Biomed. Mater. Res., Part A*, 2005, **73**, 339–348.
28 W. Sokolowski, A. Metcalfe, S. Hayashi, L. Yahia and J. Raymond, *Biomed. Mater.*, 2007, **2**, 23–27.
29 M. Behl, M. Y. Razzaq and A. Lendlein, *Adv. Mater.*, 2010, **22**, 3388–3410.
30 J. Leng, H. Lu and S. Du, in *Shape-Memory Polymers and Multifunctional Composites*, ed. J. Leng and S. Du, CRC Press, 2010, pp. 133–201.
31 H. Koerner, G. Price, N. A. Pearce, M. Alexander and R. A. Vaia, *Nat. Mater.*, 2004, **3**, 115–120.
32 J. W. Cho, J. W. Kim, Y. C. Jung and N. S. Goo, *Macromol. Rapid Commun.*, 2005, **26**, 412–416.
33 N. G. Sahoo, Y. C. Jung, H. J. Yoo and J. W. Cho, *Compos. Sci. Technol.*, 2007, **67**, 1920–1929.
34 Y. J. Liu, H. B. Lv, X. Lan, J. S. Leng and S. Y. Du, *Compos. Sci. Technol.*, 2009, **69**, 2064–2068.
35 S. A. Madbouly and A. Lendlein, in *Adv. Polym. Sci.*, ed. A. Lendlein, Springer, Berlin Heidelberg, 2010, vol. 226, pp. 41–95.
36 J. Leng, X. Lan, Y. Liu and S. Du, *Prog. Mater Sci.*, 2011, **56**, 1077–1135.
37 H. Meng and G. Li, *Polymer*, 2013, **54**, 2199–2221.
38 G. Fei, C. Tuinea-Bobe, D. Li, G. Li, B. Whiteside, P. Coates and H. Xia, *RSC Adv.*, 2013, **3**, 24132–24139.
39 A. M. Schmidt, *Macromol. Rapid Commun.*, 2006, **27**, 1168–1172.
40 T. Weigel, R. Mohr and A. Lendlein, *Smart Mater. Struct.*, 2009, **18**, 025011.
41 M. Y. Razzaq, M. Behl and A. Lendlein, *Adv. Funct. Mater.*, 2012, **22**, 184–191.
42 A. Lendlein and R. Langer, *Science*, 2002, **296**, 1673–1676.
43 A. Lendlein and S. Kelch, *Mater. Sci. Forum*, 2005, **492–493**, 219–224.
44 N. Y. Choi, S. Kelch and A. Lendlein, *Adv. Eng. Mater.*, 2006, **8**, 439–445.
45 Y. S. Wong, Y. Xiong, S. S. Venkatraman and F. Y. C. Boey, *J. Biomater. Sci., Polym. Ed.*, 2008, **19**, 175–191.
46 Y. L. Wang, Y. G. Li, Y. F. Luo, M. N. Huang and Z. Q. Liang, *Mater. Lett.*, 2009, **63**, 347–349.
47 K. Nagahama, Y. Ueda, T. Ouchi and Y. Ohya, *Biomacromolecules*, 2009, **10**, 1789–1794.
48 L. L. Liu and W. Cai, *Mater. Lett.*, 2009, **63**, 1656–1658.
49 L. Xue, S. Dai and Z. Li, *Biomaterials*, 2010, **31**, 8132–8140.
50 J. Kunzelman, T. Chung, P. T. Mather and C. Weder, *J. Mater. Chem.*, 2008, **18**, 1082–1086.
51 Y. Wu, J. Hu, H. Huang, J. Li, Y. Zhu, B. Tang, J. Han and L. Li, *J. Polym. Sci., Part B: Polym. Phys.*, 2014, **52**, 104–110.
52 M. Ecker and T. Pretsch, *RSC Adv.*, 2014, **4**, 286–292.
53 D. C. MacLaren and M. A. White, *J. Mater. Chem.*, 2003, **13**, 1695–1700.
54 D. C. MacLaren and M. A. White, *J. Mater. Chem.*, 2003, **13**, 1701–1704.
55 D. C. MacLaren and M. A. White, *J. Mater. Sci.*, 2005, **40**, 669–676.
56 A. Seeboth and D. Lötzsch, in *Thermochromic phenomena in polymers*, Smithers Rapra Technology Limited, Shrewsbury, England, 2008, pp. 17–21.
57 A. Seeboth and D. Lötzsch, in *Thermochromic and Thermotropic Materials*, Pan Stanford Publishing Pte. Ltd., Singapore, 2014, pp. 67–77.
58 F. Müller, W. Bräuer, K. H. Ott and H. G. Hoppe, EP Pat., EP0571830B1, 1993.
59 N. Fritzsche and T. Pretsch, in *Proceedings of the ASME Conference on Smart Materials, Adaptive Structures and Intelligent Systems*, 2012, vol. 1, pp. 81–88.
60 U. Siemann, in *Scattering Methods and the Properties of Polymer Materials*, Springer, Berlin Heidelberg, 2005, vol. 130, pp. 1–14.
61 ISO/IEC 18004:2000(E), *Information technology - Automatic identification and data capture techniques - Bar code symbology - QR Code*, Geneva, Switzerland, 2000.
62 Barcode Generator, http://www.barcode-generator.org.
63 ImageJ, http://rsbweb.nih.gov/ij/.
64 A. A. Michelson, in *Studies in Optics*, The University of Chicago Press, Chicago, Illinois, 1927, pp. 36–41.

65 T. Pretsch, M. Ecker, M. Schildhauer and M. Maskos, *J. Mater. Chem.*, 2012, **22**, 7757–7766.
66 ZXing, http://code.google.com/p/zxing/.
67 T. Pretsch, I. Jakob and W. Müller, *Polym. Degrad. Stab.*, 2009, **94**, 61–73.
68 G. Jimenez, N. Ogata, H. Kawai and T. Ogihara, *J. Appl. Polym. Sci.*, 1997, **64**, 2211–2220.
69 T. D. Fornes and D. R. Paul, *Polymer*, 2003, **44**, 3945–3961.
70 X. X. Zhang, Y. F. Fan, X. M. Tao and K. L. Yick, *J. Colloid Interface Sci.*, 2005, **281**, 299–306.
71 R. Kulčar, M. Friškovec, N. Hauptman, A. Vesel and M. K. Gunde, *Dyes Pigments*, 2010, **86**, 271–277.
72 S. Lakio, J. Heinamaki and J. Yliruusi, *AAPS PharmSciTech*, 2010, **11**, 46–53.
73 M. Ecker and T. Pretsch, *Smart Mater. Struct.*, 2013, **22**, 094005.
74 CIE 15.3:2004, *Colorimetry*, Vienna, Austria, 2004.
75 DIN 5033-1:2009-05, *Basic terms of colorimetry*, Berlin, Germany, 2009.
76 R. Kulčar, M. Friškovec, M. K. Gunde and N. Knešaurek, *Color. Technol.*, 2011, **127**, 411–417.
77 G. Mie, *Ann. Phys.*, 1908, **25**, 377–445.
78 M. Ecker and T. Pretsch, in *Materials Challenges and Testing for Manufacturing, Mobility, Biomedical Applications and Climate*, ed. W. Udomkichdecha, T. Böllinghaus, A. Manonukul and J. Lexow, Springer, Berlin Heidelberg, 2014, pp. 25–35.